Structure
Resource

Using a Combined Computational-Experimental Approach to Predict Antibody-Specific B Cell Epitopes

Inbal Sela-Culang,[1] Mohammed Rafii-El-Idrissi Benhnia,[2,6,7] Michael H. Matho,[3] Thomas Kaever,[2] Matt Maybeno,[2] Andrew Schlossman,[2] Guy Nimrod,[1] Sheng Li,[4] Yan Xiang,[5] Dirk Zajonc,[3] Shane Crotty,[2] Yanay Ofran,[1,8,*] and Bjoern Peters[2,8,*]

[1]The Goodman Faculty of Life Sciences, Nanotechnology Building, Bar Ilan University, Ramat Gan 52900, Israel
[2]Division of Vaccine Discovery, La Jolla Institute for Allergy and Immunology, La Jolla, CA 92037, USA
[3]Division of Cell Biology, La Jolla Institute for Allergy and Immunology, La Jolla, CA 92037, USA
[4]Medicine and Biomedical Sciences Graduate Program, University of California at San Diego, La Jolla, CA 92093, USA
[5]Department of Microbiology and Immunology, University of Texas Health Science Center, San Antonio, TX 78229, USA
[6]Present address: Department of Biochemistry and Molecular Biology and Immunology, University of Seville Medical School, 41009 Seville, Spain
[7]Present address: Laboratory of Immunovirology, Biomedicine Institute of Seville, Infectious Diseases Service, Virgen del Rocío University Hospital, 41013 Seville, Spain
[8]These authors contributed equally to this work
*Correspondence: yanay@ofranlab.org (Y.O.), bpeters@liai.org (B.P.)
http://dx.doi.org/10.1016/j.str.2014.02.003

SUMMARY

Antibody epitope mapping is crucial for understanding B cell-mediated immunity and required for characterizing therapeutic antibodies. In contrast to T cell epitope mapping, no computational tools are in widespread use for prediction of B cell epitopes. Here, we show that, utilizing the sequence of an antibody, it is possible to identify discontinuous epitopes on its cognate antigen. The predictions are based on residue-pairing preferences and other interface characteristics. We combined these antibody-specific predictions with results of cross-blocking experiments that identify groups of antibodies with overlapping epitopes to improve the predictions. We validate the high performance of this approach by mapping the epitopes of a set of antibodies against the previously uncharacterized D8 antigen, using complementary techniques to reduce method-specific biases (X-ray crystallography, peptide ELISA, deuterium exchange, and site-directed mutagenesis). These results suggest that antibody-specific computational predictions and simple cross-blocking experiments allow for accurate prediction of residues in conformational B cell epitopes.

INTRODUCTION

B cell, or antibody (Ab), epitopes hold the key for understanding antigenic interactions. They are also instrumental in many applications such as vaccine design, disease prevention, diagnostics, and therapy (Yang and Yu, 2009). Correct identification of epitopes can reveal the molecular effect of Abs on their antigens (Ags). It is also potentially useful for biotechnological applications, e.g., by allowing the use of epitopes as diagnostic reagents to replace potentially pathogenic complete Ags or as immunogens for raising Abs or for vaccination. Existing methods for identification of B cell epitopes (such as X-ray crystallography, pepscan, phage display, expressed fragments, partial proteolysis, mass spectrometry, and mutagenesis analysis) not only are expensive, laborious, and time consuming but also fail to identify many epitopes (Xu et al., 2010). Moreover, many of these methods typically identify linear stretches as epitopes, while, arguably, most of the epitopes on protein Ags are conformational and even discontinuous. While X-ray crystallography is maybe the most reliable technique for epitope identification (Sun et al., 2011), it is expensive, time consuming, and very difficult to apply for many targets. Recently, deuterium exchange mass spectrometry (DXMS) has been used to identify epitopes (Coales et al., 2009; Malito et al., 2013; Obungu et al., 2009; Pandit et al., 2012; Zhang et al., 2011a); however, this technology, which has thus far been mastered only by a handful of laboratories, requires advanced expertise and expensive equipment. Moreover, the performance of this technology in the task of epitope mapping has not been systematically assessed to determine the false-positive and false-negative rates.

For over 30 years, researchers have tried to predict Ab epitopes (Hopp and Woods, 1981). Broadly speaking, current prediction approaches attempt to predict the location of epitopes based on the presence of features associated with Ab binding sites, such as hydrophilicity and protrusion from the surface of the Ag (Ambroise et al., 2011; Ansari and Raghava, 2010; Kulkarni-Kale et al., 2005; Liang et al., 2009, 2010; Ponomarenko et al., 2008; Rubinstein et al., 2009a, 2009b; Sun et al., 2009; Sweredoski and Baldi, 2008; Zhang et al., 2011b). While tools for T cell epitope prediction are commonly used to guide experimental studies (Vita et al., 2010), existing Ab epitope prediction methods are not widely used, and several independent assessments have concluded that most of them are not sufficiently accurate to be of much practical value (Blythe and Flower, 2005; Ponomarenko and Bourne, 2007).

The comparison of Ab and T cell epitope prediction methods is instructive, as the success of the latter is due to a key difference: commonly utilized T cell epitope prediction methods do not examine Ags for general features associated with T cell

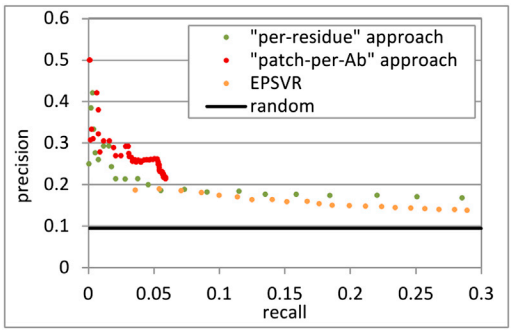

Figure 1. Epitope Prediction Performance for Published 3D Structures of Ab:Ag Complexes

The figure depicts a PRC. The performances of the per-residue approach, the patch-per-Ab approach, and the EPSVR method are shown in green, red, and orange dots, respectively. The random precision is shown as a black line. Note that the leftmost dot of the PRC for the EPSVR predictions corresponds to the highest score that can be obtained from the EPSVR website, corresponding to its highest possible precision.

See also Figure S1 and Tables S1 and S6.

recognition. Rather, different predictions are made, which are dependent on the specific major histocompatibility complex (MHC) molecule binding and presenting the epitope to T cells (Liang et al., 2010). We hypothesized that a similarly more restrictive approach can be useful in predicting Ab epitopes and propose a paradigm shift: instead of asking what parts of an Ag can be bound by any Ab induced by this Ag, we propose to predict the epitope of a given Ab using that Ab's sequence and to identify a surface patch on the Ag that has complimentary features to that specific Ab.

It has been shown that protein-protein interfaces differ in their characteristics (e.g., amino acid composition) from the rest of the protein surface (Chakrabarti and Janin, 2002; Jones and Thornton, 1997a, 1997b; Keskin et al., 2008; Lo Conte et al., 1999; Ofran and Rost, 2003), allowing their a priori identification from structure and even from sequence (de Vries and Bonvin, 2008; Ofran, 2009). B cell epitopes, however, are virtually indistinguishable from Ag surface residues in general (Kringelum et al., 2013; Kunik and Ofran, 2013; Lollier et al., 2011), hampering identification based on their intrinsic characteristics (Kringelum et al., 2013; Ponomarenko and Bourne, 2007). However, the propensity of a certain type of amino acid to contact another amino acid is different in Ab:Ag interfaces from the propensity in other protein-protein interfaces (Kunik and Ofran, 2013). These preferences could not help in identifying epitopes in general, but they may help in determining whether a given Ab with a given set of complementary determining regions (CDRs) is likely to bind a certain epitope.

Clearly, incorporation of relevant experimental data into the prediction scheme is expected to improve the predictions. This is particularly appealing in cases where it is possible to use results that are easy to obtain and do not require laborious and expensive procedures. Our suggested approach of predicting Ab-specific epitopes lends itself to such incorporation with experimental results of a cross-blocking assay between all Abs of a given Ag. While other epitope prediction methods cannot straightforwardly utilize such data to improve predictions, these data can be readily applied to the approach we suggest here and dramatically improve the prediction of epitopes.

Here, we present an Ab-specific epitope prediction approach and show its performance for a representative set of Ab:Ag complexes. We then apply this approach to predicting epitopes in the D8 protein of the vaccinia virus (VACV), a prominent target of neutralizing Abs elicited by the smallpox vaccine. Using several different experimental methods, we mapped four different epitopes for 12 Abs of this Ag. While our computational method performs better than one of the best state-of-the-art classic epitope prediction methods, additional increase in the prediction performance was achieved by incorporating experimental cross-blocking results. Unless otherwise specified, we use the terms "mapping" or "identification" to refer to experimental characterization of residues or patches that contact the paratope. The term "prediction" refers to computational suggestion of epitopic residues.

RESULTS

Derivation of an Ab-Specific Epitope Prediction Algorithm

We set out to determine what properties are associated with Ab:Ag interfaces. We extracted all structures of Ab:Ag complexes from the Protein Data Bank (PDB) and compiled a nonredundant set of 120 structures (Experimental Procedures; Table S1 available online). For a given Ab:Ag complex in this set, we identified all possible pairs of residues in the CDRs of the Ab and on the surface of the Ag. Of the total 1,779,229 pairs of CDR:Ag surface residues, 6,605 are in contact and 1,772,624 (99.6%) are not. Using this data set of interface residues, we could identify properties associated with Ab:Ag residues that are in direct contact versus those that are not. In addition, the preference of a certain amino acid to bind another amino acid was assessed based on their respective propensities in the Ab:Ag interface residues data set (Experimental Procedures; Figures S1A and S1B). Next, we trained the "Random-Forest" (RF) machine-learning algorithm (Breiman, 2001) to predict the propensity of a given residue in an Ab CDR to contact a given residue on the Ag surface, based on the properties of those residues (Experimental Procedures; Figure S1C). For each Ag residue, the features included surface accessibility, secondary structure, predicted disorder, predicted interaction hotspots, the amino acid considered, and amino acids neighboring in sequence. For each Ab residue, the features included the location in the Ab (given as heavy or light chain; CDR 1, 2 or 3; and the residue position within the CDR), the amino acid considered, and amino acids neighboring in sequence. Finally, the likelihood of the Ab and Ag residues to pair up (based on the contact potential; Experimental Procedures; Figures S1A and S1B) is considered as a feature as well. It is important to note that all these features can be calculated from the sequence of the Ab and Ag and do not require 3D structure.

The RF model assigns a "pair score" to each CDR:Ag residue pair, ranging from 0 (pairs confidently predicted not to bind) to 1 (pairs confidently predicted to bind). For each Ag residue, its highest pair score was considered as the "residue score" (RS), representing its predicted probability of being in contact with any of the Ab residues (i.e., to be in the epitope). Figure 1 shows

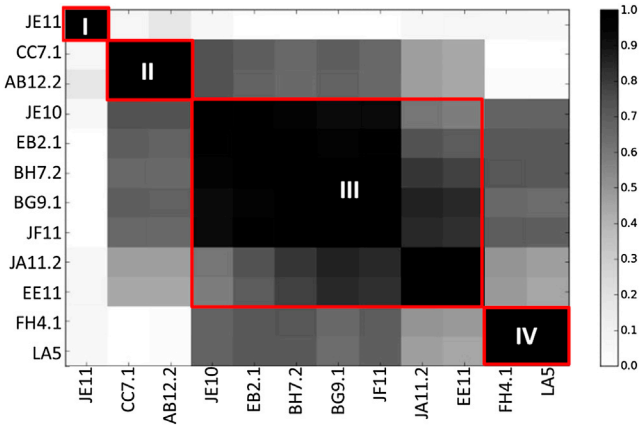

Figure 2. Cross-Blocking of D8 Abs

Black cells correspond to Abs that block D8 binding of each other and are thus assumed to share overlapping epitopes. Gray cells correspond to Abs that partially blocked each other. Empty cells correspond to Abs that did not affect the D8 binding of each other. The four groups of Abs are indicated by red boxes. See also Table S2.

a precision-recall curve (PRC) evaluating the performance of this "per-residue" prediction approach in green. Every point represents the precision and recall of the prediction at a given RS cutoff (Experimental Procedures). The PRC shows the typical tradeoff between these two measures, where higher precision is obtainable at the expense of lower recall and vice versa. The precision of the prediction is consistently above random, indicated by a black line in Figure 1.

As a reference, we also calculated the PRC for EPSVR (Figure 1, orange), an epitope prediction method recently shown to represent the best state-of-the-art structure-based epitope prediction methods (Ambroise et al., 2011; Liang et al., 2010; Yao et al., 2013; Zhang et al., 2011b). The per-residue approach outperforms EPSVR, particularly in the range of high precision. While EPSVR requires knowledge of the Ag 3D structure, the per-residue approach outperforms it in a mode of operation that does not require it. Thus, while the improvement may seem small, it actually allows for much wider applicability for any Ag that was not solved experimentally. Moreover, about 20% of the Ab:Ag complex structures in the test set were included in the EPSVR training set (while none of them were included in the training set of the per-residue approach). It is important to note that this traditional prediction method does not take into account the Ab sequence for which a prediction is made; thus, its task is inherently different. Nevertheless, juxtaposing these PRC graphs demonstrates the contribution of the information found in the Ab sequence.

To further improve our prediction method, we took advantage of the fact that epitope residues are not randomly scattered along the primary protein sequence but are rather clustered together on the 3D surface of an Ag. This may improve the precision by allowing the identification of predictions that are clustered together in patches on the protein surface. Technically, we incorporated this into our prediction approach by computing a "patch score" (PS) of a given Ag residue, which simply averaged its RS with that of its four closest neighboring surface residues. The PS was used to select the best five-residue patch for each Ag, and each residue within this patch was predicted to be in contact if its RS was above a selected cutoff score. The size of the patch affects the precision and recall of the predictions. To achieve high precision, we selected a patch size of five residues. A larger patch size would result in a higher recall and lower precision, as demonstrated in Figure S1D. The PRC of this "patch-per-Ab" approach is shown in Figure 1, in red. For a given recall, the corresponding precision of the patch-per-Ab approach was higher than that of the per-residue approach and that of EPSVR. As expected, the prediction performance is better for small Ags (<100 amino acids) than for large ones (>400 amino acids), while this effect of Ag size is diminished as the precision is increased (Figure S1E). We further evaluated the prediction performance by applying the algorithm to an external test set of all Ab:Ag complexes that were solved after the algorithm was generated and that are not similar to any of the Ags in the main data set (22 complexes). The performance on this external test set was similar to that of the main test set (Figure S1F).

For subsequent predictions, we used the patch-per-Ab approach and selected an RS cutoff of 0.43; i.e., only residues of the best patch of an Ab:Ag complex, which have an RS > 0.43, are predicted to be in the corresponding epitope. This RS cutoff score corresponds to a recall of 0.05 and a precision of 0.26 and was selected since the precision decreased significantly for lower RS cutoff scores. Recall of 0.05 at the residue level is large enough to provide at least one correctly predicted epitope residue for 43% of the Ab:Ag pairs in the data set. Thus, for 43% of the Ags in the data set, residues in the highest scoring patch were part of the epitope.

Practical Application of the Prediction Algorithms to the VACV Ag D8

As part of the National Institutes of Health immunomics roadmap (Sette et al., 2005), we have worked on identifying epitopes recognized by Abs elicited by the smallpox vaccination. To test the performance of the prediction algorithms in a practical application, we utilized a set of murine monoclonal Abs (Meng et al., 2011) specific to the D8 Ag in the VACV, the active component of the smallpox vaccine. D8 is a VACV surface protein targeted by neutralizing Abs, and we were not aware of any epitopes mapped in this Ag as our study began. This makes D8 a biologically relevant and truly blind test case for our prediction method. We sequenced each Ab and found that several Abs isolated from the same animal had highly related sequences, presumably because they had common progenitors. Using the CDR prediction approach from Kunik et al. (2012a), we found that our panel contained Abs with 12 combinations of CDRs (Table S2). Using cross-blocking assays, we found that the Abs cluster into at least four distinct groups (Figure 2), so that Abs of the same group show the same pattern of cross-blocking for all Abs in the other groups and thus are assumed to share the same, or very close, epitopes. Abs in groups I, II, and IV do not block each other's binding. However, Abs from group III can block the binding of group II and IV Abs, which may be explained by partially overlapping binding regions or by adjacent epitopes that cause steric hindrances. This panel of Abs and experimental information represents a typical starting point for an epitope mapping study. Therefore, we utilized it in combination with our prediction approach (discussed later).

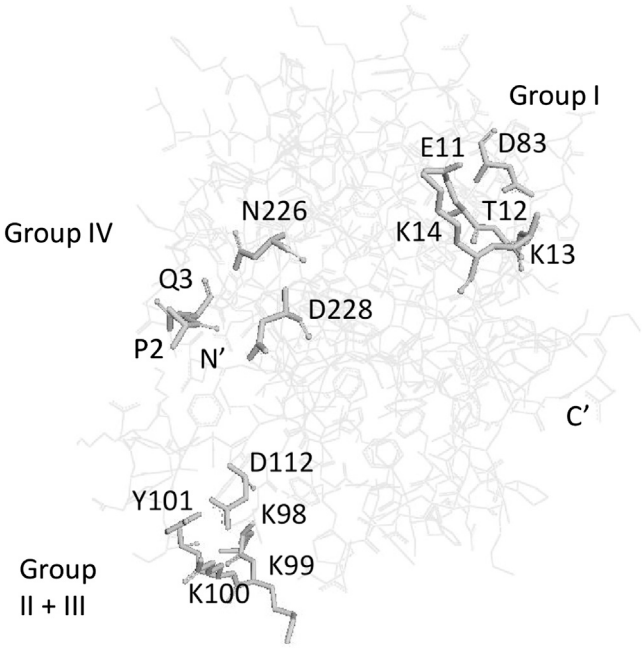

Figure 3. Projection of the Patch-per-Group Predictions on the D8 Structure

Predicted residues are presented as sticks. The N′ and C′ termini are labeled. See also Table S3.

We applied three prediction approaches to this set of Abs. First, we predicted the epitopes of all anti-D8 Abs using EPSVR. We then used the patch-per-Ab approach described earlier to provide Ab-specific predictions. Finally, we integrated the cross-blocking results into our predictions using a ''patch-per-group'' approach. In this approach, the cross-blocking data are used on two levels. First, we divide the Abs into groups, so that all the Abs in one group cross-block each other. We then predict one patch for each group, as all Abs in a group are assumed to bind the same (or a very similar) epitope. This is done by generating an ''average epitope'' for the group, where each residue is scored by averaging the raw residue score for that residue over all Abs in the group. Then, the clustering method described in the patch-per-Ab approach is applied to the ''average epitope,'' resulting in a set of putative patches for each group, ranked by their score (see Experimental Procedures for details). This way, residues that are predicted to have a high score for several Abs within one group are preferred over those that have a high score for fewer Abs. The second level utilizes information from Abs that belong to different cross-blocking groups: Abs from two groups that did not cross-block each other's binding are unlikely to bind residues that are close in space (let alone the same residue), while Abs from two groups that partially cross-block each other are unlikely to bind distant residues. Importantly, we prioritize the groups of cross-blocking Abs according to the number of Abs in each group. We first make a prediction for the group with the highest number of cross-blocking Abs, as it is the group for which we have more independent pieces of experimental evidence and thus it is expected to yield the most reliable predictions. Then, we make a prediction for the group with the second largest number of Abs, by selecting the predicted patch with the highest score from among the patches that agree with the cross-blocking results. This is done repeatedly for all groups, so that the newly predicted patch is in agreement with all selected patches of the previous groups.

Figure 3 presents the projection of the residues predicted by the patch-per-group approach on to the D8 structure (the predicted residues of each group are also listed in Table S3). Analyzing these results structurally suggests that the epitopes for group II and group III Abs overlap substantially. As shown in Figure 2, Abs from groups II and III partially blocked each other. The cross-blocking results also show that group IV Abs partially blocked group III but did not block group I Abs. However, the patch predicted for group IV does not seem to be closer to the patch predicted for group III than to the patch predicted for group I. This may suggest that the actual epitope of group III (and not of group II) extends beyond the predicted residues toward the predicted patch for group IV.

Experimental Epitope Mapping of Anti-D8 Abs

To map epitopes of the Abs in our test set, we first performed ELISAs using 20-mer peptides overlapping by 10 residues and spanning the D8 Ag (i.e., sliding window of 20 positions with step size of 10). The results are shown in Figure 4A: Abs from both group II and group III recognized a linear peptide spanning residues 91–110. A significantly higher signal was obtained for group II Abs. Truncation analysis of the peptide showed that the binding site was contained in residues 93–110 (data not shown). To fine-map the binding site, we performed alanine substitutions of peptide 93–110 and tested peptides with substitutions for their ability to block the binding of the Abs to the wild-type peptide 91–110. As shown in Figure 4B, this revealed two distinct binding patterns for the group II Abs versus the tested group III Abs.

Next, we performed crystallization trials with Abs from all groups. For the group IV Abs, we succeeded in determining a high-resolution structure of the LA5 Ab in complex with the D8 protein, along with apo structures of the D8 Ag and the LA5 Ab (Matho et al., 2012). The solved crystal structure of the D8:LA5 complex allowed us to locate the 93–110 peptide and its alanine scanning results, relative to group IV epitope, in the 3D space (Figure 4C). The residues important for the binding of groups II and III Abs are clustered into two intersecting regions, suggesting two partially overlapping epitopes. This is in agreement with the cross-blocking results, according to which these two groups of Abs compete with each other. Moreover, the residues important for group III Abs are closer to the LA5 binding site than those important for group II. Indeed, two of the three residues that are important for group III but not for group II Abs binding (Y104 and K108) are also included in the group IV epitope. This provides an explanation of why group IV Abs compete with group III but not with group II Abs, while both group II and III Abs bound the same linear peptide.

Finally, we performed deuterium exchange experiments with the JE11 Ab (group I), for which none of the other methods succeeded in revealing the epitope (Experimental Procedures). Figure 4D shows that the regions corresponding to residues 10–14 and 80–90 have the most slowing of deuterium exchange in the presence of group I Ab (an average slowdown over the three time points of 24.1% and 23.3%, respectively). As shown in Figure 4E, these two linear sequence regions come together in the D8 protein to form a contiguous binding surface.

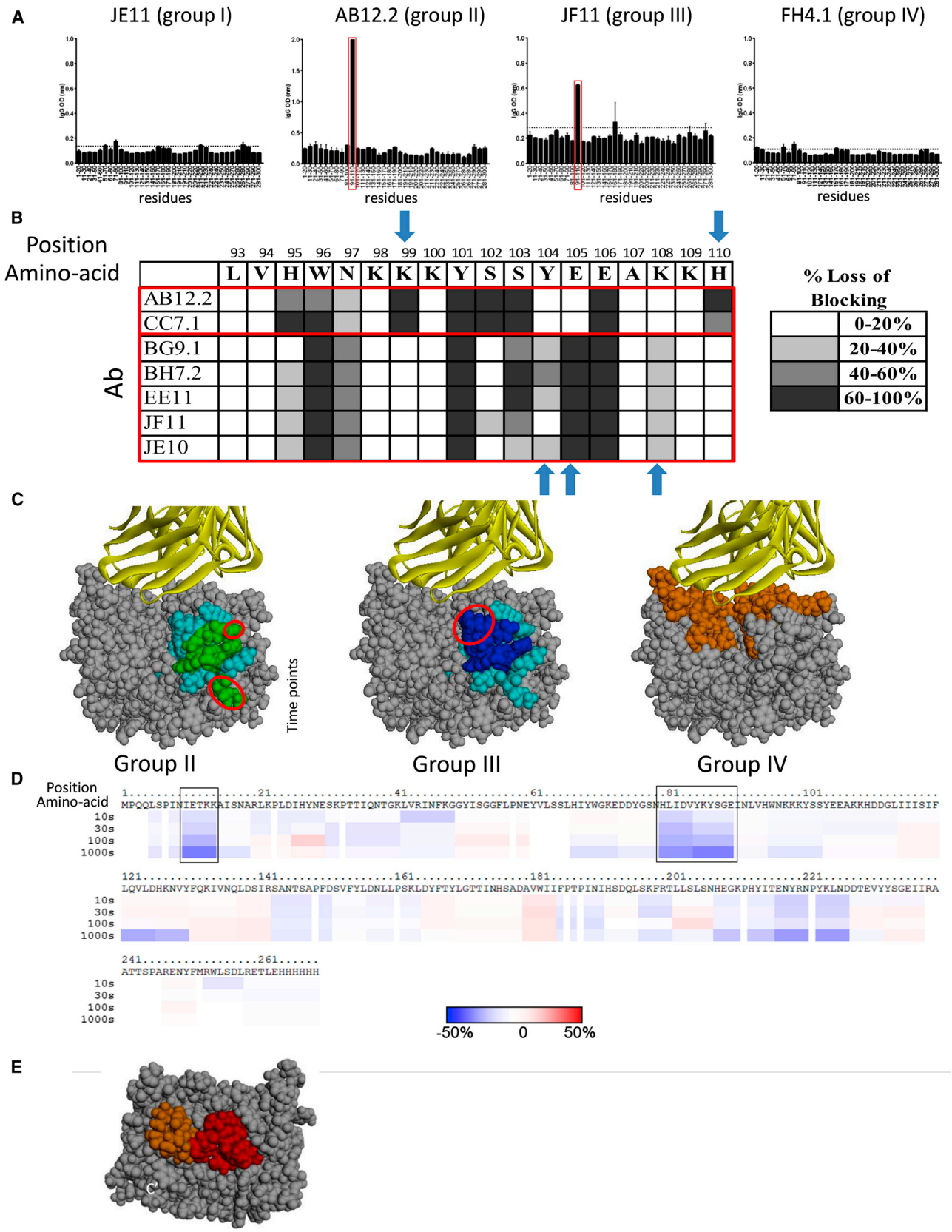

(legend on next page)

Validation of Identified Epitopes Using Site-Directed Mutagenesis

To further confirm the epitopes we have identified, we produced 13 variants of D8 in which individual residues were mutated to an alanine and tested how these single amino acid substitutions affected the binding ability of one representative Ab per group in ELISAs. The binding of these variants and their location are shown in Figures 5 and S2. Eleven variants were picked based on the mutated residue being in the epitopes as inferred from the experimental epitope mapping. Six of these variants indeed showed a significant drop in binding of all Abs of the group that binds the epitope that includes the mutated residues, but not in binding of Abs from other groups, emphasizing the role of these residues in Ab binding. Three variants did not affect binding of any of the Abs, despite the fact that the residues were spatially located within the respective binding sites. Finally, two variants (Y101A and E106A) showed little binding for any of the Abs, suggesting that the mutations may have misfolded the proteins or hampered their stability. Two additional mutants (K211A and D25A), which were not mapped to any of the four epitopes, were picked as a negative control and indeed did not affect D8 binding to any of the tested Abs. Overall, these data confirm our epitope mapping results and provide additional details on which residues contribute most to the binding affinity.

Evaluation of Prediction Performance for Anti-D8 Abs

Figure 6A indicates the predicted epitopes together with the epitopes we identified experimentally (Experimental Procedures; Table S4). The epitope of group I covers all five residues in the predicted patch of that group. The epitope of group IV covers two of the four predicted residues for this group. The 93–110 peptide, which represents group II and III epitopes, covers all four residues predicted for group II and three of the four residues predicted for group III. The one residue from group III not included in the 93–110 peptide is D112 (dark blue). Mutation of D112 to alanine suggests that it affects the binding of group II Abs (Figure 5A) but does not affect the binding of Abs from group III or any of the other groups.

We evaluated our D8 epitope predictions made with the patch-per-Ab and patch-per-group strategies and EPSVR in a quantitative fashion as well. Figure 6B shows that the use of competition binding data leads to a better recall as well as precision and, ultimately, to the elimination of most false-positive predictions.

For further evaluation of the patch-per-group approach, we applied it to lysozyme, since it has the largest number of solved structures bound to different Abs. This allowed us to divide the nine Abs that bind the lysozyme into four groups based on the spatial location of their epitopes on the lysozyme surface. To apply the patch-per-group approach, we assumed that Abs within each of these four groups are likely to cross-block each other based on their relative location. We found that the patch-per-group approach resulted in an almost 2-fold increase in precision over the patch-per-Ab approach, similar to the improvement observed for D8 (Table S5). While the transformation from the multiple X-ray structures to the ''assumed'' cross-blocking matrix is not trivial, this provides another example for the power of using several Ab-specific predictions together with competition data to improve performance.

DISCUSSION

The present study evaluates an Ab epitope prediction approach on both a comprehensive data set of crystal structures from the PDB and a set of Abs targeting the VACV D8 protein. For the latter, we have combined multiple experimental approaches to map epitopes and validate the predictions. Linear peptide epitope mapping studies are often criticized for missing conformational epitopes and, therefore, introducing bias in the space of known epitopes. However, crystallization trials of Ab:Ag complexes also often fail for various reasons. This might also introduce biases when relying solely on epitopes identified in crystallization studies. To reduce bias, it is necessary to map the epitopes of all Abs for a given target, as we demonstrated here by using multiple experimental approaches. We suggest that this experimental approach of combining multiple epitope mapping techniques is advantageous over any single approach, as different techniques succeed for different Abs, and the information gained from different experiments complement each other to gain a fuller understanding of Ab:Ag interactions.

The current standard approach to B cell epitope prediction is to scan an Ag for determinants that possess physicochemical or structural traits similar to those observed in known epitopes. Independent benchmark studies have concluded that the performance of tools based on this approach is not impressive (Blythe and Flower, 2005; Ponomarenko and Bourne, 2007). Several technical and computational limitations have been suggested to explain the poor performance of this standard approach (Greenbaum et al., 2007; Ponomarenko and Bourne, 2007). These methods attempt to predict the epitopes on a given Ag for any Ab. However, almost any residue on the Ag surface may be a

Figure 4. Experimental Epitope Mapping

(A) ELISA assessment of D8 peptides binding to the Abs. Peptide 91–110 (red box) bound group II and III Abs but not group I and IV Abs. Error bars indicate SEMs based on duplicate values.

(B) Alanine scan for peptide 93–110. Residue positions that, when substituted for alanine, abrogated binding of the peptide to the corresponding Ab (black cells), residue positions that reduced but did not abrogate binding (gray cells), and positions that had no effect on binding (empty cells). The upper red rectangle represents group II Abs, and the lower red rectangle represents group III Abs. Upper arrows indicate peptide residues that were important only for group II Abs binding, and lower arrows indicate positions that were important only for group III Abs binding.

(C) 3D structure of D8 bound to LA5 Ab (group IV). Residues that abrogated binding in alanine scan are shown in green for group II (left) and dark blue for group III (middle). Residues that exclusively affected binding of Abs from one group but not the other are circled. Residues of the 93–110 linear peptide that did not affect binding of either group II or group III Abs are highlighted in cyan. The group IV epitope residues are colored orange (right). The LA5 Ab is shown in a yellow ribbon representation.

(D) Differences in deuteration levels in the presence compared to absence of Ab binding at four time points. Slower deuterium exchange is marked in blue, and a faster exchange is marked in red. Residues 10–14 and 80–90 (black box) show the most marked slowing.

(E) The 10–14 and 80–90 peptides are shown in orange and red, respectively, on the D8 structure.

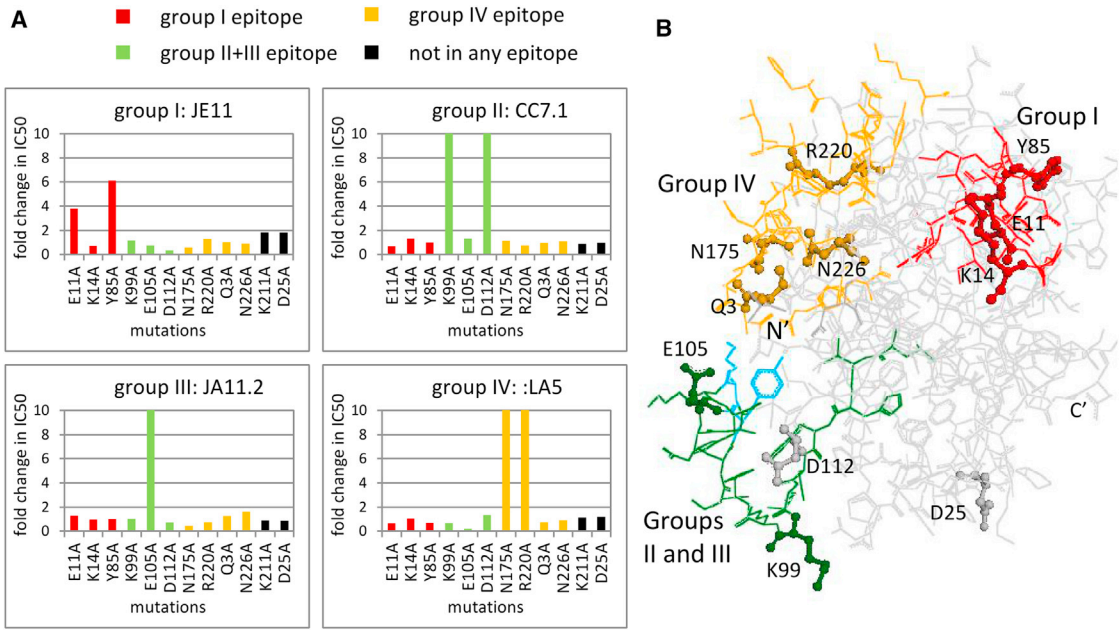

Figure 5. Site-Directed Mutagenesis

(A) Summary of all titration curves. Half maximal inhibitory concentration (IC_{50}) values were extrapolated using the Prism Software package. The bar graphs indicate the fold change in IC_{50} value for a given mutant protein and a given Ab compared to the median IC_{50} values of that Ab/mutant protein, as calculated by median polishing. For example, the group I Ab JE11 has an IC_{50} value of 17 ng/ml for the mutant E11A, while its median IC_{50} value over all the mutant and wild-type measurements is 3 ng/ml, which is an ~6-fold difference. Mutated residues that were mapped to the epitope of group I, II + III, and IV Abs are shown as dark red, green, and orange bars, respectively. Mutated residues that were not mapped to any of the epitopes are shown as black bars.

(B) The mutated residues in the context of the D8 structure. Epitope residues of group I (inferred from the DXMS assay), group II and III (inferred from the ELISA), and group IV (as observed in the D8:LA5 crystal structure) are colored red, dark green, and orange, respectively. Y104 and K108, which are common to the group IV epitope and the 93–110 peptide (group II and III epitopes), are colored light blue. The mutated residues are shown in ball-and-stick representation. K211 is not shown as it is disordered in the D8 crystal structure.

See also Figure S2.

part of an epitope of some Abs. (Benjamin et al., 1984; Greenbaum et al., 2007; Novotný et al., 1986; Thornton et al., 1986). Thus, many of the false-positive predictions of this approach might actually be epitopic residues of an Ab that is yet to be characterized (Sela-Culang et al., 2013). This is especially true when only a small number of Abs of a certain Ag are available. The alternative methodology we suggest here is based on earlier studies of the Ofran lab, which suggested a change of perspective: rather than classifying Ag residues a priori as epitopic or nonepitopic, we predict the potential match between a given Ab and a given epitope.

We improved performance by incorporating structural information to define epitopes as residue patches on the Ag (the patch-per-Ab approach). The most significant improvement in prediction performance was achieved by including the experimental cross-blocking data and making predictions for groups of Abs (the patch-per-group approach). While the cross-blocking data were required in order to reach the high performance showed in the D8 case, the experimental cross-blocking results themselves (without the computational method) are not of much use for epitope mapping. Moreover, the cross-blocking data could be utilized only with a computational method that predicts an epitope of a given Ab (as opposed to the "classical" approach that predicts an epitope for any Ab). Thus, it is the combination of the Ab-specific epitope prediction approach and the cross-blocking experiment that allowed for this performance.

One of the features we used to train the machine learning is an amino acids pairing preferences matrix (Figures S1A and S1B). While many amino acids showed high preferences for other amino acids of the same type (e.g., hydrophobic-hydrophobic) or of opposite charge (e.g., positive-negative), there are also some preferences of hydrophobic amino acids for hydrophilic ones. Such preferences in Ab:Ag recognition have been mentioned in the past (Blalock and Bost, 1986; Blalock and Smith, 1984; Bost and Blalock, 1989).

One limitation of our method is that it only allows us to predict patches of amino acid residues that are likely to be located within a discontinuous epitope recognized by a given Ab of known sequence. This does not amount to an accurate identification of the entire epitope, which typically consists of many more residues that contribute to its overall antigenic or immunogenic specificity. How would these patches be useful for the design of diagnostic tools and vaccines? We may consider the predicted patch as an "anchor" to the entire epitope. This anchor may be then used as a starting point for revealing the rest of the epitope. For example, mutating several residues near the anchor but in different directions may lead to the right direction to which the anchor extends. Furthermore, the cross-blocking data may sometimes provide additional information in this regard. In the D8 case, for example, both group II and III Abs shared partially overlapping anchors, while only group III

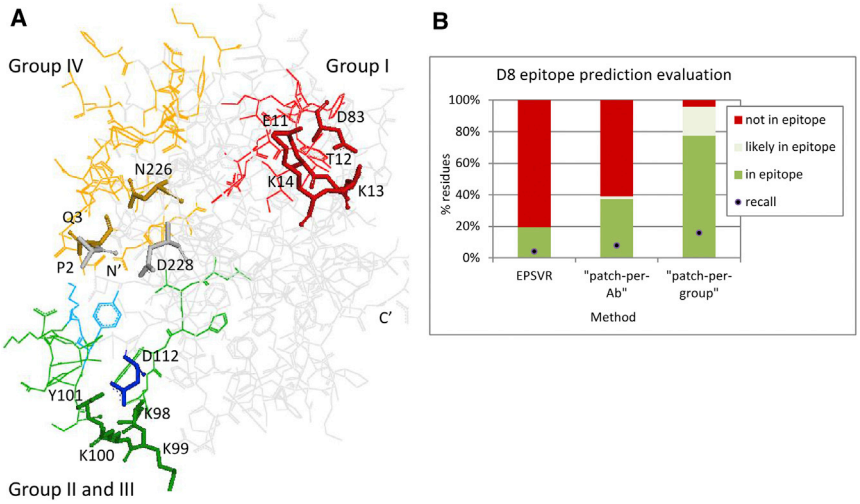

Figure 6. D8 Epitope Prediction Evaluation

(A) Qualitative evaluation: the observed epitope of group I (inferred from the DXMS assay), group II and III (inferred from the ELISA), and group IV (as observed in the D8:LA5 crystal structure) are colored red, dark green, and orange, respectively. D112, which is considered a part of group II epitope based on the mutagenesis results, is colored dark blue. Y104 and K108, which are common to the group IV epitope and the 93–110 peptide (group II and III epitopes), are colored light blue. The predicted residues based on the patch-per-group approach are shown as sticks, while all other residues are shown as lines.

(B) Quantitative evaluation: The percentage of the predicted residues that are, indeed, in the epitope (true-positive), those that are likely to be in the epitope, and those that are not in the epitope (false-positive) are represented in dark green, light green, and red bars, respectively (see Experimental Procedures for the different definitions). The percentage of epitope residues predicted as such (recall) is indicated with black dots. Results are shown for predictions made with the patch-per-Ab and patch-per-group approaches and with the EPSVR method.

See also Tables S4 and S5.

Abs compete with the Abs of group IV. Thus, a reasonable assumption would be that the epitope of group III Abs is further extended toward that of group IV, while the epitope of group II is extended to a different direction.

Another limitation is that our epitope predictions in their current form are not immediately applicable to identify either potential diagnostic reagents or immunogens capable of inducing a broad immune response, as in both cases, it is not a single binding specificity found in one Ab that is relevant but a variety of different Ab molecules that may be implicated. Instead, our methodology is primarily relevant to identifying the epitopes of existing sets of monoclonal Abs. There are, however, scenarios in which the identification of the binding site of one Ab is important. For example, in studying the effect of a broadly neutralizing Ab or using such Abs to design a general vaccine, one would want to identify the epitope of that specific Ab. Similarly, the attempts to develop monoclonal Abs for various applications often require the mapping of specific epitopes. Moreover, we believe that our approach may also constitute an important step toward more general design of diagnostic reagents and immunogens, which can, for example, be achieved by scaling up the number of Ab sequences considered based on next-generation sequencing and expanding the prediction approach by integrating this information. Future studies will need to experimentally validate that this will be feasible.

Our Ab epitope prediction approach performs better than existing approaches but also requires additional experimental data to be applicable. Existing Ab epitope prediction approaches only require the Ag sequence and/or structure as an input. In addition, our approach requires the sequence of the binding Ab. Current sequence information is available nearly exclusively for Abs with a known crystal structure. This is probably due to the historic difficulty of determining Abs sequences with standard sequencing techniques due to the variability of the Ab coding genes. This has been only recently overcome by the emergence of sequencing approaches using Ab primer cocktails (Casellas et al., 2007; Ehlers et al., 2006; Wang et al., 2000). Thus, the availability of Ab sequences should no longer be a bottleneck for future prediction studies. To fully take advantage of the approach, the 3D structure of the Ag is also needed, as well as a set of Abs and their cross-blocking pattern. For the 3D structure, since both the secondary structure and surface accessibility features can be predicted from sequence, the per-residue approach is readily applicable to any Ag, even when there is no experimentally determined 3D structure available. The patch-per-Ab and patch-per-group approaches, which take into account the spatial location of the Ag residues, require an experimentally determined 3D structure of the Ag or of a close homolog. For the availability of sets of Abs and cross-blocking data, all studies that we are aware of, aimed at producing monoclonal Abs against a target, start out with a set of candidate Abs that is subsequently narrowed down to candidates with the most desirable properties. It should, therefore, be possible in most studies to generate cross-blocking data and to sequence Abs, even if the epitope from only one Ab is of interest. Thus, our approach for Ab epitope prediction is applicable to most practical applications where a set of Abs for a target has already been generated.

Several possible avenues exist to further improve the prediction quality of an Ab-specific binding prediction approach. First, it will likely be possible to improve prediction performance by optimizing the specific machine-learning algorithm approach utilized and by adding to the features used to determine whether or not a given Ab:Ag residue pair is in contact. The data set included in the present study provides a benchmark set for others to develop and evaluate such potential improvement in methodology. Second, a current bottleneck is the availability of high-quality experimental data. The most valuable data are fully resolved 3D structures of Ab:Ag complexes. When we assembled our data set from the PDB, there were 646 complexes of Ags with human or murine Abs available. However, only 120 complexes had unique Ab:Ag pairs. This means that, on average, each Ab:Ag combination is represented by more than five experimentally determined structures. To truly understand Ab:Ag contact

preferences, more unique Ab:Ag complexes of physiological relevance are needed. This call for more representative structures is similar to the needs identified in the structural genomics initiative (Burley et al., 1999). While it is unlikely that a plethora of new Ab:Ag crystal structures will be available in the near future, simply because crystal structures remain very hard to obtain, a realistic near-term goal is that the amino acid sequences of monoclonal Abs with known epitopes are published as part of their characterization and are thereby deposited in the Immune Epitope Database (Vita et al., 2010).

Finally, while the patch-per-Ab approach was optimized using a training set and tested on an independent test set, the patch-per-group approach could not be trained and tested in a similar way, since we are not aware of systems in which the cross-blocking data of different Abs, as well as their epitopes on a common Ag, are known. Instead, the patch-per-group procedure was built based on a simple logic and applied for the D8 case study, followed by experimental mapping of the different epitopes. Thus, some parameters, such as the Abs grouping procedure, may have been done differently. For example, group III appears to be composed of two subsets of Abs, where the Abs in each subset completely cross-block each other but only partially cross-block the Abs in the other subset. The likely structural interpretation is that there are two overlapping epitopes. By grouping these two subsets together, we allow a more accurate identification of the residues that are common to both of these epitopes. This gives us higher precision for the residues we identify. When more cases with available cross-blocking and epitopes data will be available, it will be possible to further optimize the procedure.

EXPERIMENTAL PROCEDURES

Computational Epitope Prediction

Data Set Construction

A nonredundant data set of Ab-Ag structures from Burkovitz et al. (2014) was used. Briefly, a list of 646 human and mouse Ab:Ag X-ray structures was extracted from IMGT/3Dstructure-DB (version 4.5.0) (Lefranc et al., 2010), and the structures were downloaded from the PDB website. Abs sequences were clustered using BLASTCLUST (Dondoshansky and Wolf, 2002), requiring 97% sequence identity and 95% coverage. A representative from each of the resulting clusters was selected based on the following criteria. First, the structure with fewest in vitro modifications was selected. Then, the structure with the longest Ag, and then the structure with the better resolution, was preferred. Structures with Ags of fewer than 65 amino acids were not included. The final data set contained 120 Ab:Ag complexes.

The data set was divided into three subsets for 3-fold cross-validation. CD-HIT (Li and Godzik, 2006) was used to cluster all structures, with Ag sequence identity >70%. Structures of the same cluster were assigned to the same subset. Thus, different Abs with the same Ag were not used both to train and to test a single RF model. The structures in each of the three subsets are listed in Table S1.

RF Model Generation

Applying the 3-fold cross-validation approach, we generated three complementary RF models, each trained on two subsets and tested on the third. For each of the structures in the training set, all pairs of residues—one from the Ab CDRs and one from the Ag surface—were extracted. The CDRs were defined using PARATOME (Kunik et al., 2012a, 2012b) in a mode of operation that requires only the sequence of the Ab. DSSP (Kabsch and Sander, 1983) was used to calculate the solvent accessibility of each of the Ag residues, and residues with a solvent accessibility >0 were defined as surface residues. For each pair of residues, the following features were extracted or calculated.

1. The paired amino acid on the Ag, four amino acids N terminal to it, and four amino acids C terminal to it.
2. The paired amino acid on the Ab, four amino acids N terminal to it, and four amino acids C terminal to it.
3. The relative solvent accessibility of the Ag residue. The DSSP value was divided by the theoretical maximal solvent accessibility of that amino acid.
4. The secondary structure of the Ag residue as calculated by DSSP (helix, strand, or loop).
5. The Ab chain (heavy or light).
6. The CDR number (1, 2, or 3).
7. The position of the Ab residue in its CDR (1 for the residue on the N-terminal end of the CDR).
8. The predicted disorder state of the Ag residue (disordered or not, as calculated by MD [Schlessinger et al., 2009]).
9. The predicted classification of the interaction hotspot for the Ag residues (a hotspot or not, as calculated by ISIS [Ofran and Rost, 2007]).
10. A pair contact potential representing the potential for the interaction between the residues at hand, calculated as described later.

Each pair of residues was labeled as positive (i.e., an observed contact) if at least two of their respective nonhydrogen atoms were within 5Å of each other or as negative (i.e., not in contact) otherwise. All 10 features of the positive pairs and of the randomly selected negative pairs, and their classification, were submitted to a 1,000 trees RF run implemented by R.

Ab:Ag Contact Potential Generation

All Ab:Ag pairs of residues in contact (within a distance of 5 Å) were extracted from the data set. For each combination of two amino acid types, i from the Ab and j from the Ag, the pair's statistical energy E_{ij} was calculated according to Equation 1, where f^{ij} is the number of times the two amino acids i and j were found to be in contact, f^i is the number of times amino acid i appears in a paratope, and f^j is the number of times amino acid j appeared in an epitope. Since there are almost no cysteines in the Ab paratopes or methionine in the light-chain CDRs, the E values of all 20 pairs of cysteine (in both chains) and of methionine (in the light chain) were not calculated.

$$E_{ij} = \log_2 \frac{\frac{f^{ij}}{\sum_{ij=1}^{400} f^{ij}}}{\frac{f^i}{\sum_{i=1}^{20} f^i} * \frac{f^j}{\sum_{j=1}^{20} f^j}} \quad (1)$$

Using the RF Model for Epitope Prediction

The RF model produced a pair-score between 0 (for pairs of residues that are predicted to not bind) and 1 (for pairs of residues predicted to be a part of the Ab:Ag interface). This score was used in two different strategies to provide a final prediction of epitopes. In the per-residue approach, the RS of an Ag residue is defined as the highest pair-score of this residue and is used for predicting individual residues to be in the epitope: for a selected RS cutoff score, all residues with an RS above this cutoff score are predicted to be in the epitope. The patch-per-Ab approach incorporates the information of predicted residues that are close in space by searching for patches of predicted epitope residues. For each Ag surface residue, the four residues closest in space were grouped together with it to generate a patch. The PS is defined as the average RS over all residues within the patch. Since all patches contain five residues, the PS is comparable. For a given Ab:Ag pair, the patch with the highest PS was selected, and the residues in this patch were predicted to be in the epitope if their RS was above a selected cutoff score. If there was more than one patch with the same PS, the one with the highest single RS was preferred.

Model Performance Evaluation

Each RF model was trained on two thirds of the available data and tested to predict the epitope residues of the Ag:Ab pairs in the remaining one third of the data as a test set. The predictions were combined on the whole set in order to evaluate the overall prediction performance. PRCs were drawn by calculating the precision and recall for different RS cutoffs. Precision and recall were defined as:

$$precision = \frac{TP}{TP + FP} \quad (2)$$

and

$$recall = \frac{TP}{TP + FN}, \quad (3)$$

where TP is the number of true-positive predictions, FP is the number of false-positive predictions, and FN is the number of false-negative predictions.

Random precision was calculated as the number of residues in all epitopes divided by the number of all Ag surface residues.

The performance of the per-residue and the patch-per-Ab strategies were compared to that of EPSVR using the EPSVR server (http://sysbio.unl.edu/EPSVR/) to predict epitopes of all 120 Ags in the data set. A score between 0 and 100 was assigned to each of the Ag residues. The prediction was assessed with respect to the epitopes in our data set.

Applying the RF Model to D8

All 120 Ag:Ab complexes were used to generate another RF model applied to D8 and its Abs. Note that no BLAST e-value of less than 0.1 was found between D8 and any of the Ags in the data set. All pairs of residues, one from the Ab CDRs and one from the D8 surface, were extracted, and their features were calculated as described. For the 12 Abs, only their sequence was used to calculate the features. For D8, the apo X-ray structure (PDB ID 4E9O) was used. MODELER (Sali et al., 1995) was used to model three residues (N207–E209) disordered in the crystal structure.

The predictions for D8 were made using the patch-per-Ab and the patch-per-group strategies described earlier.

In the patch-per-Ab strategy, the patch with the highest PS was selected, and if two or more patches with the same PS existed, the one with the single best RS was preferred. As described in the Results section, residues in the best patch with an RS above 0.43 were predicted to be in the epitope.

In the patch-per-group strategy, each Ag surface position was assigned a group residue score (GRS), which is the average of all RSs assigned to this position by the corresponding Abs in the group. Then the group PS (GPS) is assigned to each Ag surface residue in complete analogy to the PS. The predictions were made for one group at a time, ordering the groups by decreasing number of Abs. First, a prediction was made to the group with the largest number of Abs, then to the second largest group, and so on. In each group, the best scoring patch was considered first. If it was not in agreement with the cross-blocking data, (i.e., it overlapped with a selected patch of another group while the Abs of these two groups do not compete with each other, or alternatively, if the patch is distant from a selected patch of another group with which it does compete), the patch was excluded for this group, and the second best patch was examined, and so on. Residues in the selected patch that have a GRS above 0.43 were considered as the final prediction.

D8 Prediction Evaluation

For each of the four groups, each Ag surface residue was defined as either "in epitope," "likely in epitope," or "not in epitope," based on the experimental data available (see Supplemental Experimental Procedures for details). LA5 is the only Ab for which we know the structure of the epitope based on the crystal structure of the Ab:Ag binding site. For the remainder of the Abs, epitopes were mapped by nonstructural assays, and we determined the residues likely to be part of the structural epitope as follows: for Ab FH4. One (group IV), we assumed that its epitope is identical to that of LA5, as they completely block each other's binding and show the same pattern in blocking the binding of all other Abs. For all Abs in groups II and III, we assumed that the residues in the 93–110 peptide are in the epitope of these Abs. While the cross-blocking and alanine scanning of the peptide suggests that these two groups have only partially overlapping epitopes (see Results), these data do not allow us to determine which residue belongs to which epitope, since a mutation of a residue that does not affect binding may still be part of the corresponding epitope. For Abs of group II, we assumed that their epitope includes D112 as well (based on the site-directed mutagenesis data). For Ab JE11 (group I), we assumed that the epitope includes residues 10–14 and 80–90 (based on the DXMS data). To make the epitope definition of groups I–III more comparable to the definition of the group IV epitope (and since residues not included in the ELISA and DXMS peptides may still be in the respective epitopes), residues within a distance of 3 Å of the residues described earlier were included in the list of putative epitope residues ("likely in epitope"). Table S4 summarizes the definitions of each of the four groups.

Applying EPSVR to D8

The EPSVR server provides a score between 0 and 100 for each Ag residue. To have the most appropriate comparison with our method, we considered for each Ab:D8 complex, the x best scored residues, where x is the number of residues predicted by the patch-per-Ab approach.

External Test Set Construction

All Ab:Ag crystal structures that were published since May 2011 were collected. Ab sequences were clustered, and a representative from each cluster was selected as described earlier in the "Data Set Construction" section. CD-HIT was then used to cluster together all Ags from the main data set and from the external test set with sequence identity > 70%. Only Ags from the external test set that were not clustered with Ags from the main data set were included in the final external test set. One structure (PDB ID code: 3SOB), for which not all CDRs were predicted by PARATOME, was excluded. The final test set contained 22 Ab:Ag pairs (see Table S6 for the full list of PDB ID codes).

External Test Set Performance

The prediction performance of the external test set was done in the same way as for the main data set. The RF model used was the one built using all 120 Ab:Ag pairs of the main data set (the same model used for the prediction of D8 epitopes). Epitopes were predicted using the patch-per-Ab approach.

Epitope Mapping by ELISA

Overlapping 20-mer peptides for the D8 Ag were synthesized and tested for Ab binding using an ELISA. Flat-bottomed 96-well microtiter plates were coated with 100 μl of NeutrAvidin biotin-binding protein (1 μg/ml) diluted in PBS overnight at 4°C (ThermoScientific Pierce). Then, coated plates were washed with washing buffer (PBS, pH 7.2, plus 0.05% Tween 20) and blocked with blocking buffer (PBS, pH 7.2, plus 1% BSA plus 0.1% Tween 20) for 2 hr at room temperature (RT). Plates were incubated with 100 μl of overlapping linear biotinylated peptides (200 ng/ml) in blocking buffer for 90 min at RT. Plates were washed and incubated with purified monoclonal Ab at 10 μg/ml for 90 min at RT. Plates were washed, and the bound Ab was detected by adding a streptavidin-horseradish peroxidase (HRP)-conjugated secondary antibody to mouse immunoglobulin G (Invitrogen) and incubated for 60 min at RT, followed by OPD substrate (Sigma-Aldrich).

Epitope Mapping by Deuterium Exchange

To maximize peptide sequence coverage, the optimized quench and proteolysis condition was determined prior to DXMS experiments (Hailey et al., 2009; Li et al., 2011). For each sample, 0.5 μl of stock solution of D8 at 4.7 mg/ml was diluted with 7.5 μl of H_2O buffer (8.3 mM Tris-HCl, 150 mM NaCl, in H_2O, pH 7.2) at 0°C and then quenched with 12 μl of a quench solution of 0.8% formic acid, 16% glycerol, and GdnHCl at final concentrations of 0.5 M and 1.0 M. The samples were then frozen on dry ice and stored at −80°C. Procedures for pepsin digestion from DXMS have been described elsewhere (Burns-Hamuro et al., 2005) (see Supplemental Experimental Procedures for details).

In addition, nondeuterated samples (incubated in H_2O buffer mentioned earlier) and equilibrium-deuterated back-exchange control samples (incubated in D_2O buffer containing 0.5% formic acid overnight at 25°C) were prepared as described elsewhere (Hamuro et al., 2004; Li et al., 2011) The centroids of the isotopic envelopes of nondeuterated, functionally deuterated, and fully deuterated peptides were measured using HDExaminer and then converted to corresponding deuteration levels with corrections for back-exchange (Zhang and Smith, 1993).

Cross-Blocking ELISA

Ag was prepared at 0.5 μg/ml and used to coat Nunc Polysorbent flat-bottomed 96-well plates with 100 μl per well. Plates were incubated overnight at 4°C and washed four times with PBS plus 0.05% Tween 20. We added 100 μl of blocking buffer (PBS + 10% fetal bovine serum) to the plate and incubated it for 90 min at room temperature. Blocking buffer was discarded, and 100 μl of antibodies of interest were added to the plate at 10 μg/ml and incubated for 90 min. HRP-conjugated antibodies of interest (Innova Biosciences Lightning-Link HRP conjugation kit) were prepared at 0.5 μg/ml and added

to the plates for 20 min. The plates were developed using o-phenylenediamine, and optical density at 490 nm was read on a SpectraMax 250 (Molecular Devices).

Peptide Truncation and Alanine Scan

Variant peptides with N- or C-terminal truncations and/or alanine substitutions were tested for their ability to block binding to their parent 20-mer peptides in an ELISA. Ninety-six-well plates were coated with 100 μl NeutrAvidin per well at a concentration of 0.5 μg/ml (see Supplemental Experimental Procedures for details).

Protein Mutagenesis

D8 variants with single-residue changes to alanine were generated by site-directed mutagenesis performed directly in the pET22b+ expression vector using the QuickChange II Site-Directed Mutagenesis Kit (by Agilent) according to manufacturer's suggestions. Successful mutations were confirmed by sequencing (see Supplemental Experimental Procedures for details).

ACCESSION NUMBERS

The Immune Epitope Database accession number for epitope mapping data reported in this paper is http://www.iedb.org/subID/1000515. The Genbank accession numbers for the antibody sequences reported in this article are AGO04750, AGO04761, KF017296, KF017307, KF017295, KF017306, KF017297, KF017308, KF017304, KF727003, KF017298, KF017309, KF017299, KF017310, KF017300, KF017311, KF017301, KF017312, KF017302, KF017313, KF017303, KF017314, JQ815182, and JQ815183.

SUPPLEMENTAL INFORMATION

Supplemental Information includes Supplemental Experimental Procedures, two figures, and six tables and can be found with this article online at http://dx.doi.org/10.1016/j.str.2014.02.003.

ACKNOWLEDGMENTS

This project has been funded in whole or in part with federal funds from the National Institutes of Allergy and Infectious Diseases under Contract no. HHSN272200900048C. Y.O. was supported in part by the Israeli Science Foundation, grant no. 511/10 (http://www.isf.org.il). We thank Anat Burkovitz for providing the data set; Shauli Ashkenazy for running the ISIS and MD programs; and Ariel Feiglin, Vered Kunik, Sivan Goren, and Ahron Brodie for their helpful comments.

Received: November 6, 2013
Revised: January 23, 2014
Accepted: February 1, 2014
Published: March 13, 2014

REFERENCES

Ambroise, J., Giard, J., Gala, J.L., and Macq, B. (2011). Identification of relevant properties for epitopes detection using a regression model. IEEE/ACM Trans. Comput. Biol. Bioinformatics *8*, 1700–1707.

Ansari, H.R., and Raghava, G.P. (2010). Identification of conformational B-cell epitopes in an antigen from its primary sequence. Immunome Res. *6*, 6.

Benjamin, D.C., Berzofsky, J.A., East, I.J., Gurd, F.R., Hannum, C., Leach, S.J., Margoliash, E., Michael, J.G., Miller, A., Prager, E.M., et al. (1984). The antigenic structure of proteins: a reappraisal. Annu. Rev. Immunol. *2*, 67–101.

Blalock, J.E., and Bost, K.L. (1986). Binding of peptides that are specified by complementary RNAs. Biochem. J. *234*, 679–683.

Blalock, J.E., and Smith, E.M. (1984). Hydropathic anti-complementarity of amino acids based on the genetic code. Biochem. Biophys. Res. Commun. *121*, 203–207.

Blythe, M.J., and Flower, D.R. (2005). Benchmarking B cell epitope prediction: underperformance of existing methods. Protein Sci. *14*, 246–248.

Bost, K.L., and Blalock, J.E. (1989). Production of anti-idiotypic antibodies by immunization with a pair of complementary peptides. J. Mol. Recognit. *1*, 179–183.

Breiman, L. (2001). Random forests. Mach. Learn. *45*, 5–32.

Burkovitz, A., Sela-Culang, I., and Ofran, Y. (2014). Large-scale analysis of somatic hypermutations in antibodies reveals which structural regions, positions and amino acids are modified to improve affinity. FEBS J. *281*, 306–319.

Burley, S.K., Almo, S.C., Bonanno, J.B., Capel, M., Chance, M.R., Gaasterland, T., Lin, D., Sali, A., Studier, F.W., and Swaminathan, S. (1999). Structural genomics: beyond the human genome project. Nat. Genet. *23*, 151–157.

Burns-Hamuro, L.L., Hamuro, Y., Kim, J.S., Sigala, P., Fayos, R., Stranz, D.D., Jennings, P.A., Taylor, S.S., and Woods, V.L., Jr. (2005). Distinct interaction modes of an AKAP bound to two regulatory subunit isoforms of protein kinase A revealed by amide hydrogen/deuterium exchange. Protein Sci. *14*, 2982–2992.

Casellas, R., Zhang, Q., Zheng, N.Y., Mathias, M.D., Smith, K., and Wilson, P.C. (2007). Igkappa allelic inclusion is a consequence of receptor editing. J. Exp. Med. *204*, 153–160.

Chakrabarti, P., and Janin, J. (2002). Dissecting protein-protein recognition sites. Proteins *47*, 334–343.

Coales, S.J., Tuske, S.J., Tomasso, J.C., and Hamuro, Y. (2009). Epitope mapping by amide hydrogen/deuterium exchange coupled with immobilization of antibody, on-line proteolysis, liquid chromatography and mass spectrometry. Rapid Commun. Mass Spectrom. *23*, 639–647.

de Vries, S.J., and Bonvin, A.M. (2008). How proteins get in touch: interface prediction in the study of biomolecular complexes. Curr. Protein Pept. Sci. *9*, 394–406.

Dondoshansky, I., and Wolf, Y. (2002). Blastclust (NCBI Software Development Toolkit). (Bethesda, MD: NCBI).

Ehlers, M., Fukuyama, H., McGaha, T.L., Aderem, A., and Ravetch, J.V. (2006). TLR9/MyD88 signaling is required for class switching to pathogenic IgG2a and 2b autoantibodies in SLE. J. Exp. Med. *203*, 553–561.

Greenbaum, J.A., Andersen, P.H., Blythe, M., Bui, H.H., Cachau, R.E., Crowe, J., Davies, M., Kolaskar, A.S., Lund, O., Morrison, S., et al. (2007). Towards a consensus on datasets and evaluation metrics for developing B-cell epitope prediction tools. J. Mol. Recognit. *20*, 75–82.

Hailey, K.L., Li, S., Andersen, M.D., Roy, M., Woods, V.L., Jr., and Jennings, P.A. (2009). Pro-interleukin (IL)-1beta shares a core region of stability as compared with mature IL-1beta while maintaining a distinctly different configurational landscape: a comparative hydrogen/deuterium exchange mass spectrometry study. J. Biol. Chem. *284*, 26137–26148.

Hamuro, Y., Anand, G.S., Kim, J.S., Juliano, C., Stranz, D.D., Taylor, S.S., and Woods, V.L., Jr. (2004). Mapping intersubunit interactions of the regulatory subunit (RIalpha) in the type I holoenzyme of protein kinase A by amide hydrogen/deuterium exchange mass spectrometry (DXMS). J. Mol. Biol. *340*, 1185–1196.

Hopp, T.P., and Woods, K.R. (1981). Prediction of protein antigenic determinants from amino acid sequences. Proc. Natl. Acad. Sci. USA *78*, 3824–3828.

Jones, S., and Thornton, J.M. (1997a). Analysis of protein-protein interaction sites using surface patches. J. Mol. Biol. *272*, 121–132.

Jones, S., and Thornton, J.M. (1997b). Prediction of protein-protein interaction sites using patch analysis. J. Mol. Biol. *272*, 133–143.

Kabsch, W., and Sander, C. (1983). Dictionary of protein secondary structure: pattern recognition of hydrogen-bonded and geometrical features. Biopolymers *22*, 2577–2637.

Keskin, O., Gursoy, A., Ma, B., and Nussinov, R. (2008). Principles of protein-protein interactions: what are the preferred ways for proteins to interact? Chem. Rev. *108*, 1225–1244.

Kringelum, J.V., Nielsen, M., Padkjær, S.B., and Lund, O. (2013). Structural analysis of B-cell epitopes in antibody:protein complexes. Mol. Immunol. *53*, 24–34.

Kulkarni-Kale, U., Bhosle, S., and Kolaskar, A.S. (2005). CEP: a conformational epitope prediction server. Nucleic Acids Res. *33* (Web Server issue), W168–W171.

Kunik, V., and Ofran, Y. (2013). The indistinguishability of epitopes from protein surface is explained by the distinct binding preferences of each of the six antigen-binding loops. Protein Eng. Des. Sel. *26*, 1–11.

Kunik, V., Ashkenazi, S., and Ofran, Y. (2012a). Paratome: an online tool for systematic identification of antigen-binding regions in antibodies based on sequence or structure. Nucleic Acids Res. *40* (Web Server issue), W521–W524.

Kunik, V., Peters, B., and Ofran, Y. (2012b). Structural consensus among antibodies defines the antigen binding site. PLoS Comput. Biol. *8*, e1002388.

Lefranc, M.P., Ehrenmann, F., and Kaas, Q. (2010). IMGT/3Dstructure-DB and IMGT/DomainGapAlign: a database and a tool for immunoglobulins or antibodies, T cell receptors, MHC, IgSF and MhcSF. Nucleic Acids Res. *38*, D301–D307.

Li, W., and Godzik, A. (2006). Cd-hit: a fast program for clustering and comparing large sets of protein or nucleotide sequences. Bioinformatics *22*, 1658–1659.

Li, S., Tsalkova, T., White, M.A., Mei, F.C., Liu, T., Wang, D., Woods, V.L., Jr., and Cheng, X. (2011). Mechanism of intracellular cAMP sensor Epac2 activation: cAMP-induced conformational changes identified by amide hydrogen/deuterium exchange mass spectrometry (DXMS). J Biol. Chem. *286*, 17889–17897.

Liang, S.D., Zheng, D.D., Zhang, C., and Zacharias, M. (2009). Prediction of antigenic epitopes on protein surfaces by consensus scoring. BMC Bioinformatics *10*, 302.

Liang, S.D., Zheng, D.D., Standley, D.M., Yao, B., Zacharias, M., and Zhang, C. (2010). EPSVR and EPMeta: prediction of antigenic epitopes using support vector regression and multiple server results. BMC Bioinformatics *11*, 381.

Lo Conte, L., Chothia, C., and Janin, J. (1999). The atomic structure of protein-protein recognition sites. J. Mol. Biol. *285*, 2177–2198.

Lollier, V., Denery-Papini, S., Larré, C., and Tessier, D. (2011). A generic approach to evaluate how B-cell epitopes are surface-exposed on protein structures. Mol. Immunol. *48*, 577–585.

Malito, E., Faleri, A., Lo Surdo, P., Veggi, D., Maruggi, G., Grassi, E., Cartocci, E., Bertoldi, I., Genovese, A., Santini, L., et al. (2013). Defining a protective epitope on factor H binding protein, a key meningococcal virulence factor and vaccine antigen. Proc. Natl. Acad. Sci. USA *110*, 3304–3309.

Matho, M.H., Maybeno, M., Benhnia, M.R., Becker, D., Meng, X., Xiang, Y., Crotty, S., Peters, B., and Zajonc, D.M. (2012). Structural and biochemical characterization of the vaccinia virus envelope protein D8 and its recognition by the antibody LA5. J. Virol. *86*, 8050–8058.

Meng, X., Zhong, Y., Embry, A., Yan, B., Lu, S., Zhong, G., and Xiang, Y. (2011). Generation and characterization of a large panel of murine monoclonal antibodies against vaccinia virus. Virology *409*, 271–279.

Novotný, J., Handschumacher, M., Haber, E., Bruccoleri, R.E., Carlson, W.B., Fanning, D.W., Smith, J.A., and Rose, G.D. (1986). Antigenic determinants in proteins coincide with surface regions accessible to large probes (antibody domains). Proc. Natl. Acad. Sci. USA *83*, 226–230.

Obungu, V.H., Gelfanova, V., Rathnachalam, R., Bailey, A., Sloan-Lancaster, J., and Huang, L. (2009). Determination of the mechanism of action of anti-FasL antibody by epitope mapping and homology modeling. Biochemistry *48*, 7251–7260.

Ofran, Y. (2009). Prediction of protein interaction sites. In Computational Protein-Protein Interactions, R. Nussinov and G. Schreiber, eds. (Boca Raton, FL: CRC Press), pp. 167–184.

Ofran, Y., and Rost, B. (2003). Analysing six types of protein-protein interfaces. J. Mol. Biol. *325*, 377–387.

Ofran, Y., and Rost, B. (2007). Protein-protein interaction hotspots carved into sequences. PLoS Comput. Biol. *3*, e119.

Pandit, D., Tuske, S.J., Coales, S.J., E, S.Y., Liu, A., Lee, J.E., Morrow, J.A., Nemeth, J.F., and Hamuro, Y. (2012). Mapping of discontinuous conformational epitopes by amide hydrogen/deuterium exchange mass spectrometry and computational docking. J. Mol. Recognit. *25*, 114–124.

Ponomarenko, J.V., and Bourne, P.E. (2007). Antibody-protein interactions: benchmark datasets and prediction tools evaluation. BMC Struct. Biol. *7*, 64.

Ponomarenko, J., Bui, H.H., Li, W., Fusseder, N., Bourne, P.E., Sette, A., and Peters, B. (2008). ElliPro: a new structure-based tool for the prediction of antibody epitopes. BMC Bioinformatics *9*, 514.

Rubinstein, N.D., Mayrose, I., Martz, E., and Pupko, T. (2009a). Epitopia: a web-server for predicting B-cell epitopes. BMC Bioinformatics *10*, 287.

Rubinstein, N.D., Mayrose, I., and Pupko, T. (2009b). A machine-learning approach for predicting B-cell epitopes. Mol. Immunol. *46*, 840–847.

Sali, A., Potterton, L., Yuan, F., van Vlijmen, H., and Karplus, M. (1995). Evaluation of comparative protein modeling by MODELLER. Proteins *23*, 318–326.

Schlessinger, A., Punta, M., Yachdav, G., Kajan, L., and Rost, B. (2009). Improved disorder prediction by combination of orthogonal approaches. PLoS ONE *4*, e4433.

Sela-Culang, I., Kunik, V., and Ofran, Y. (2013). The structural basis of antibody-antigen recognition. Front. Immunol. *4*, 302.

Sette, A., Fleri, W., Peters, B., Sathiamurthy, M., Bui, H.H., and Wilson, S. (2005). A roadmap for the immunomics of category A-C pathogens. Immunity *22*, 155–161.

Sun, J., Wu, D., Xu, T.L., Wang, X.J., Xu, X.L., Tao, L., Li, Y.X., and Cao, Z.W. (2009). SEPPA: a computational server for spatial epitope prediction of protein antigens. Nucleic Acids Res. *37* (Web Server issue), W612–W616.

Sun, P., Chen, W., Huang, Y., Wang, H., Ma, Z., and Lv, Y. (2011). Epitope prediction based on random peptide library screening: benchmark dataset and prediction tools evaluation. Molecules *16*, 4971–4993.

Sweredoski, M.J., and Baldi, P. (2008). PEPITO: improved discontinuous B-cell epitope prediction using multiple distance thresholds and half sphere exposure. Bioinformatics *24*, 1459–1460.

Thornton, J.M., Edwards, M.S., Taylor, W.R., and Barlow, D.J. (1986). Location of 'continuous' antigenic determinants in the protruding regions of proteins. EMBO J. *5*, 409–413.

Vita, R., Zarebski, L., Greenbaum, J.A., Emami, H., Hoof, I., Salimi, N., Damle, R., Sette, A., and Peters, B. (2010). The immune epitope database 2.0. Nucleic Acids Res. *38* (Database issue), D854–D862.

Wang, Z., Raifu, M., Howard, M., Smith, L., Hansen, D., Goldsby, R., and Ratner, D. (2000). Universal PCR amplification of mouse immunoglobulin gene variable regions: the design of degenerate primers and an assessment of the effect of DNA polymerase 3′ to 5′ exonuclease activity. J. Immunol. Methods *233*, 167–177.

Xu, X., Sun, J., Liu, Q., Wang, X., Xu, T., Zhu, R., Wu, D., and Cao, X. (2010). Evaluation of spatial epitope computational tools based on experimentally-confirmed dataset for protein antigens. Chin. Sci. Bull. *55*, 2169–2174.

Yang, X.D., and Yu, X.L. (2009). An introduction to epitope prediction methods and software. Rev. Med. Virol. *19*, 77–96.

Yao, B., Zheng, D., Liang, S., and Zhang, C. (2013). Conformational B-cell epitope prediction on antigen protein structures: a review of current algorithms and comparison with common binding site prediction methods. PLoS ONE *8*, e62249.

Zhang, Z., and Smith, D.L. (1993). Determination of amide hydrogen exchange by mass spectrometry: a new tool for protein structure elucidation. Protein Sci. *2*, 522–531.

Zhang, Q., Willison, L.N., Tripathi, P., Sathe, S.K., Roux, K.H., Emmett, M.R., Blakney, G.T., Zhang, H.M., and Marshall, A.G. (2011a). Epitope mapping of a 95 kDa antigen in complex with antibody by solution-phase amide backbone hydrogen/deuterium exchange monitored by Fourier transform ion cyclotron resonance mass spectrometry. Anal. Chem. *83*, 7129–7136.

Zhang, W., Xiong, Y., Zhao, M., Zou, H., Ye, X.H., and Liu, J. (2011b). Prediction of conformational B-cell epitopes from 3D structures by random forests with a distance-based feature. BMC Bioinformatics *12*, 341.